



ARL-MR-1007 • SEP 2019



Effect of Titanium (Ti)-Seed and In Vacuo Process Flow on Sputtered Lead Zirconate Titanate Thin Films

by Daniel M Potrepka, Robert R Benoit, Ryan Q Rudy, Jeffrey S Pulskamp, Glen R Fox, Christopher Y Cheng, and Susan Trolier-McKinstry

Approved for public release; distribution is unlimited.

NOTICES

Disclaimers

The findings in this report are not to be construed as an official Department of the Army position unless so designated by other authorized documents.

Citation of manufacturer's or trade names does not constitute an official endorsement or approval of the use thereof.

Destroy this report when it is no longer needed. Do not return it to the originator.



Effect of Titanium (Ti)-Seed and In Vacuo Process Flow on Sputtered Lead Zirconate Titanate Thin Films

Daniel M Potrepka, Robert R Benoit, Ryan Q Rudy, and Jeffrey S Pulskamp

Sensors & Electron Devices Directorate, CCDC Army Research Laboratory

Glen R Fox

Fox Materials Consulting LLC

Christopher Y Cheng and Susan Troler-McKinstry

Department of Materials Science and Engineering, Pennsylvania State University

REPORT DOCUMENTATION PAGE

Form Approved
OMB No. 0704-0188

Public reporting burden for this collection of information is estimated to average 1 hour per response, including the time for reviewing instructions, searching existing data sources, gathering and maintaining the data needed, and completing and reviewing the collection information. Send comments regarding this burden estimate or any other aspect of this collection of information, including suggestions for reducing the burden, to Department of Defense, Washington Headquarters Services, Directorate for Information Operations and Reports (0704-0188), 1215 Jefferson Davis Highway, Suite 1204, Arlington, VA 22202-4302. Respondents should be aware that notwithstanding any other provision of law, no person shall be subject to any penalty for failing to comply with a collection of information if it does not display a currently valid OMB control number.

PLEASE DO NOT RETURN YOUR FORM TO THE ABOVE ADDRESS.

1. REPORT DATE (DD-MM-YYYY) September 2019		2. REPORT TYPE Memorandum Report		3. DATES COVERED (From – To) 1 October 2017–30 August 2019	
4. TITLE AND SUBTITLE Effect of Titanium (Ti)-Seed and In Vacuo Process Flow on Sputtered Lead Zirconate Titanate Thin Films				5a. CONTRACT NUMBER	
				5b. GRANT NUMBER	
				5c. PROGRAM ELEMENT NUMBER	
6. AUTHOR(S) Daniel M Potrepka, Robert R Benoit, Ryan Q Rudy, Jeffrey S Pulskamp, Glen R Fox, Christopher Y Cheng, and Susan Trolier-McKinstry				5d. PROJECT NUMBER	
				5e. TASK NUMBER	
				5f. WORK UNIT NUMBER	
7. PERFORMING ORGANIZATION NAME(S) AND ADDRESS(ES) CCDC Army Research Laboratory ATTN: FCDD-RLS-RL Aberdeen Proving Ground, MD 21005.				8. PERFORMING ORGANIZATION REPORT NUMBER ARL-MR-1007	
9. SPONSORING/MONITORING AGENCY NAME(S) AND ADDRESS(ES)				10. SPONSOR/MONITOR'S ACRONYM(S)	
				11. SPONSOR/MONITOR'S REPORT NUMBER(S)	
12. DISTRIBUTION/AVAILABILITY STATEMENT Approved for public release; distribution is unlimited.					
13. SUPPLEMENTARY NOTES ORCID ID(s): Daniel Potrepka, 0000-0002-0528-1038; Robert Benoit, 0000-0002-3728-6706					
14. ABSTRACT In a process improvement study to optimize a platinum (Pt) bottom electrode for lead zirconate titanate (PZT) film growth, PZT thin films were grown on Pt bottom electrodes on thermally oxidized silicon substrates. The PZT depositions on Pt were made with no underlying layer, a nucleation layer, a titanium (Ti)-seed layer, or a combination of nucleation on Ti-seed layer. X-ray diffraction and electrical characterization determined that a Ti-seed deposited on top of the Pt, rather than on a PZT nucleation layer, was critical to produce PZT with preferred {001} orientation while minimizing secondary phases. Best electrical performance was characterized by a dielectric constant $\epsilon = 1150 \pm 100$, $\tan \delta = 0.019 \pm 0.001$ at $E = 0$, and maximum polarization of $34.7 \pm 0.6 \mu\text{C}/\text{cm}^2$ at 200 kV/cm. In contrast, characterizations performed also indicate that exclusion of the Ti-seed from the PZT stack process results in dominant diffraction peaks that appear to be generated by a pyrochlore or highly strained 110 PZT phase with pinned domains.					
15. SUBJECT TERMS sputter, lead zirconate titanate, PZT, lead zirconate titanate, thin films, X-ray diffraction, scanning electron microscopy, SEM, piezoMEMS, ferroelectric					
16. SECURITY CLASSIFICATION OF:			17. LIMITATION OF ABSTRACT SAR	18. NUMBER OF PAGES 37	19a. NAME OF RESPONSIBLE PERSON Daniel M Potrepka
a. REPORT Unclassified	b. ABSTRACT Unclassified	c. THIS PAGE Unclassified			19b. TELEPHONE NUMBER (Include area code) (301) 394-0389

Standard Form 298 (Rev. 8/98)
Prescribed by ANSI Std. Z39.18

Contents

List of Figures	iv
List of Tables	iv
Acknowledgments	v
1. Introduction	1
2. Experimental	2
2.1 X-Ray Diffraction and Analysis	6
2.2 Scanning Electron Microscopy	6
2.3 Wafer Processing and Capacitance, Polarization and Leakage Measurements	6
3. Discussion	7
3.1 X-ray Diffraction Analysis	7
3.2 SEM Image Analysis	7
3.3 Electrical Capacitance, Polarization, and Leakage Current Analyses	13
4. Conclusion	14
5. References	15
Appendix A. X-ray Diffraction Figures	17
Appendix B. Electrical-Measurement Figures	21
List of Symbols, Abbreviations, and Acronyms	27
Glossary	29
Distribution List	30

List of Figures

Fig. 1	Process steps for sputtered Ti (converted to TiO ₂), platinum (Pt), and PZT	1
Fig. 2	SEM of 1-12084 volume-only PZT layer on Pt 111 at 15k× magnification	10
Fig. 3	SEM of 6-12181 nucleation-only layer on Pt 111 at 15k× magnification	10
Fig. 4	SEM of nucleation on a) as-deposited and b) annealed Ti seed at 35k× magnification	11
Fig. 5	SEM of volume-PZT/nucleation bilayer on a) as-deposited and b) annealed Ti seed, Samples 4-12172 and 3-12077, respectively, at 35k× magnification	12

List of Tables

Table 1	Process information for sputtering of samples processed.....	5
Table 2	XRD and electrical analyses	9

Acknowledgments

We wish to acknowledge Beth Jones of Pennsylvania State University for her assistance with the X-ray diffraction measurements. This work was supported in part by The Center for Nanoscale Science, a Materials Research Science and Engineering Center supported by the National Science Foundation under grant DMR-1420620. Christopher Cheng was supported by the National Defense Science & Engineering Graduate Fellowship Program.

1. Introduction

Thin-film $\text{PbZr}_{1-x}\text{Ti}_x\text{O}_3$ (lead zirconate titanate [PZT]) is an important material in piezoelectric microelectromechanical systems (piezoMEMS) for RF devices,¹ ink-jet printer heads,² microrobotics,³ energy harvesters,⁴ and other applications. PZT films can be grown by numerous methods; of these, chemical solution deposition and sputtering both allow large-area thick films to be prepared. The sputtering process offers high throughput in manufacturing environments, but both the target stoichiometry and process conditions must be carefully controlled to achieve reproducible PZT phase purity, texture, and density.

As the piezoelectric properties are a strong function of film orientation,⁵ multiple methods have been utilized to control the nucleation of the perovskite phase.⁶⁻⁷ One approach to achieving $\{100\}$ -oriented perovskite growth is seeding the PZT with a titanium dioxide (TiO_2) film.⁸ A reproducible process was obtained by sputtering PZT onto the TiO_2 seed layer without removing the TiO_2 -coated wafer from the evacuated Evatec Clusterline deposition system where the processes were performed, as shown in Fig. 1. This implies that all steps must be completed serially with the same deposition tool, precluding ex-situ characterization of the individual stack layers and limiting process control of the individual layers. Earlier work has demonstrated that the PZT $\{001\}$ peaks are enhanced by over a factor of 10 when the titanium (Ti)-seed anneal is completed in the lead oxide (PbO)-rich environment of the Evatec Clusterline PZT chamber employing a hot chuck instead of annealing in a Tystar tube furnace.⁹

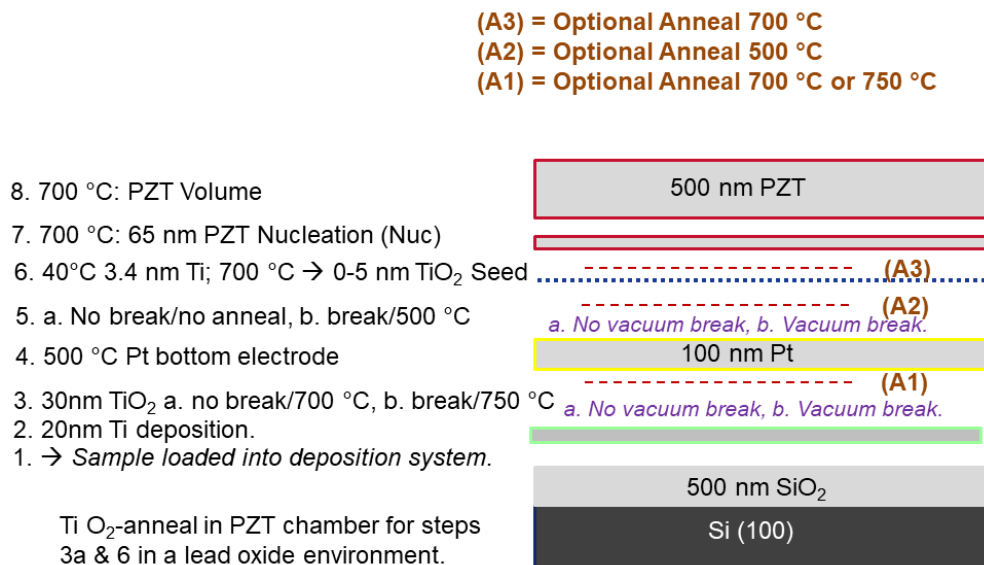


Fig. 1 Process steps for sputtered Ti (converted to TiO_2), platinum (Pt), and PZT

While the reported process enables reproducible films, it is not clear whether natural process interruption points, before and after bottom electrode deposition, could be introduced without detrimentally affecting the sputtered PZT film quality. Of particular interest is whether or not it is critical to retain a clean surface on the {111}-textured Pt bottom electrode that has not been exposed to a clean room atmosphere. In the PZT stack in-vacuum process, individual layer surface exposure to air was avoided for the bottom Pt electrode, Ti-seed, PZT nucleation, and PZT layers. Therefore, an investigation of the effects of vacuum breaks at various process points is needed to understand whether and how vacuum breaks impact PZT stack properties. Because earlier XRD studies of *in vacuo* processed PZT stacks revealed a strong effect of the Ti-seed-on-perovskite phase formation and orientation,⁹ it was of interest to characterize the phase and orientation dependence on process flows that involved sample exposure to air at some process steps (in particular, after Pt deposition). Assessment of air exposure and other factors influencing the PZT process reproducibility for {100}-textured perovskite PZT is expected to reveal how to achieve higher electromechanical performance in piezoMEMS device applications.

PZT films were produced by sputtering a Ti-seed layer, a PZT nucleation layer, and the volume layer (majority thickness or body) of the PZT film. The PZT nucleation and volume layers were sputtered using the same target, but different process conditions were employed. Various vacuum breaks and anneals at convenient interruption points in the process allowed the films to be analyzed by X-ray diffraction (XRD) and scanning electron microscopy (SEM). The XRD peaks were fit using a Pearson VII function to allow for quantification of peak intensities, positions, and widths, which enabled correlation to the process conditions. The position and intensity of high-intensity peaks with a high signal-to-noise ratio could be quantified by direct fitting of the collected data. However, low-intensity peaks were smoothed with a Savitsky–Golay filter prior to fitting. Non-perovskite, PZT-related peaks and their relationship to synthesis and PZT quality are discussed. Polarization, capacitance, and leakage measurements were performed to assess PZT film quality. The impact of vacuum breaks on film quality is also assessed.

2. Experimental

An Evatec (Oerlikon) Clusterline 200 multichamber sputtering system with Ti, Pt, and PZT targets was used for thin-film deposition. The deposition process of the Ti and Pt bottom electrode layers is based on that described by Fox et al.¹⁰ Referring to Fig. 1, a commercial wafer with 500 nm of silicon dioxide (SiO₂) on [100]-oriented silicon (Si) was loaded into the deposition system. Then, 20 nm of hexagonal, {0001}-textured Ti was sputtered onto the SiO₂ using a cathode power

of 0.5 kW, substrate temperature of 40 °C, argon (Ar) flow rate of 30 sccm, and deposition time of 35 s. To convert the Ti to 32 nm of {100}-textured rutile TiO₂, two anneal methods were used. The first *in vacuo* method retained the wafer under deposition chamber vacuum, while the second ex-situ method allowed the removal of the wafer to cleanroom and subsequent anneal furnace atmosphere conditions. All of the temperatures reported for processes in the vacuum system are nominal temperatures, measured for the chuck by a local temperature probe. In the ex-situ method, wafers were removed from the vacuum system and furnace annealed at 750°C, oxygen (O₂) at 3 SLM for 30 min.

In the *in vacuo* method, selected wafers remained in the Clusterline tool (no vacuum break) and the O₂ anneal was performed in the PZT chamber at a nominal substrate temperature of 700 °C, with a flow of 10 sccm of O₂ for 250 s. After wafer transfer under vacuum to the Pt chamber, 100 nm of {111}-textured Pt was sputtered onto the TiO₂ at a cathode power of 0.5 kW, substrate temperature of 500 °C, and Ar gas flow rate of 50 sccm for a deposition time of 67 s. For the ex-situ process, the wafers were exposed to a cleanroom atmosphere; when reintroduced to the Clusterline 200, an optional anneal of the Pt surface was performed under a vacuum of approximately 10⁻⁷ mbar at 500 °C in the Pt chamber. Next, an optional Ti-seed layer was deposited at a cathode power of 0.5 kW, substrate temperature of 40 °C, and Ar gas flow of 30 sccm for a deposition time of 3 s. An optional oxygen anneal was performed (in the PZT chamber) on selected samples held at 700 °C, in 10 sccm of flowing O₂ for 250 s to obtain a 3- to 5-nm-thick TiO₂ layer. Next, an approximately 50-nm-thick sputtered PZT nucleation layer was deposited from a Pb_{1.2}Zr_{0.52}Ti_{0.48}O₃ (PZT) target using an RF (13.6 MHz) cathode power of 2 kW, substrate temperature of 700 °C, and sputter time of 60 s. Sputtering commenced after a 60-s pump down to approximately 10⁻⁷ mbar, Ar flow at 80 sccm for 60 s to stabilize pressure, and a plasma strike at 0.5 kW cathode power. After deposition of the PZT nucleation layer, the plasma was extinguished and using the same conditions as described previously, a second pump down, gas flow stabilization, and plasma strike were employed to initiate the deposition of a 450-nm PZT (volume) film. The PZT volume film was sputtered from the PZT target using a 2-kW cathode power, 700 °C substrate temperature, and 5-s time intervals alternating between gas flows of 1) 56 sccm of Ar and 2) a mixture of 54 sccm of Ar and 4 sccm of O₂ cycled successively 67 times for a total deposition time of 670 s. Finally, a set of depositions was performed to obtain nucleation-only, PZT volume-only, and PZT-on-nucleation films, all deposited on the Pt/TiO₂ using a fully *in vacuo* process (i.e., no vacuum break at the Pt deposition step). All PZT depositions used the Evatec matching-capacitor parameters of 500 steps for C series and 900 steps for C shunt and a RF bias DC voltage of 70 V. PZT thickness was obtained using a JA Woollam ellipsometer.

Sample preparation description and sequence of events are further detailed in Table 1. The name for each sample ID and starting substrate are stated in the table. All samples received the same standard Ti deposition (Ti-1 Dep) as noted. Anneal 1 indicates whether the Ti-1 anneal was performed in the PZT chamber or the samples removed from the sputtering chamber (Vacuum Break) to anneal the Ti in the tube furnace. All samples received the same standard Pt sputter deposition (Pt-1 Dep). Vacuum breaks were made before and after the platinum deposition (Pt-1 dep) for Samples 20, 21, 19, and 18. PtB in their sample names refers to these vacuum breaks near the Pt deposition. An anneal (Anneal 2) in the Pt chamber is indicated for Samples 20 and 21. The next four columns indicate whether a Ti-seed deposition (Ti-2 Dep), Ti-seed anneal (Anneal 3), nucleation layer (N), and PZT volume (V) film (nonzero thicknesses) were deposited. Finally, the last column indicates that all samples with volume PZT were then capped with 100-nm sputter-deposited Pt (Pt-2 Dep) using the same sputtering procedures as for the bottom electrode. At this point, the XRD measurements were performed. After that, the wafers were processed to obtain arrays of electrical capacitors of area $1.0 \times 10^{-3} \text{ cm}^2$ (diameter = 357 μm). Evaporated gold (Au)/Pt/chromium (Cr) layers with thicknesses of 730/20/20 nm were then deposited on top of the Pt top electrodes for probe contact. At this point, the polarization (PE), capacitance (CV), and leakage (IV) measurements were performed to obtain figures of merit for characterizing the PZT device performance: polarization at a maximum voltage (P_{max}), dielectric constant (ϵ), loss tangent ($\tan \delta$), and leakage currents ($I(+)$ and $I(-)$), respectively. All measurements made using applied positive voltage to the top electrode and ground to the bottom electrode.

Table 1 Process information for sputtering of samples processed

(X = Yes) Sample ID	Name	Substrate	Standard Ti-1 Dep	Titanium Anneal 1	Vacuum Break	Platinum Pt-1 Dep	Vacuum Break	Platinum Anneal 2	Ti-Seed (S) Ti-2 Dep	Ti-Seed Anneal 3	Nucleation (N)	PZT Vol. (V) t (Å)	Platinum Pt-2 Dep
1-12084	V	SiO ₂	X	PZT chamber	...	Standard	4082.6	Standard
6-12181	N	SiO ₂	X	PZT chamber	...	Standard	X (~300 Å)	0	...
15-11831	V/N	SiO ₂	X	PZT chamber	...	Standard	X	11172	Standard
5-12175	V/S	SiO ₂	X	PZT chamber	...	Standard	X	5047.5	Standard
2-12174	V/S(A)	SiO ₂	X	PZT chamber	...	Standard	X	PZT chamber	...	4556.6	Standard
4-12172	V/N/S	SiO ₂	X	PZT chamber	...	Standard	X	...	X	4816	Standard
3-12077	V/N/S(A)	SiO ₂	X	PZT chamber	...	Standard	X	PZT chamber	X	4843	Standard
20-12367	V/N/S(A)/ PtB(A)	SiO ₂	X	Tube Furnace	X	Standard	X	Pt chamber	X	PZT chamber	X	4772.9	Standard
21-12195	V/N/S/PtB(A)	SiO ₂	X	Tube furnace	X	Standard	X	Pt chamber	X	...	X	4734	Standard
19-11865	V/N/S/PtB	SiO ₂	X	Tube furnace	X	Standard	X	...	X	...	X	4805.6	Standard
18-11873	V/N/S(A)/PtB	SiO ₂	X	Tube furnace	X	Standard	X	...	X	PZT chamber	X	4867.5	Standard

2.1 X-Ray Diffraction and Analysis

The XRD scans were performed on a PANalytical 4-Circle XPert3 diffractometer with Cu K α source and monochromator over a range of $10^\circ \leq 2\theta \leq 90^\circ$. Jade 7 peak fitting software was employed with Pearson VII fits to individual peaks. Peaks were fitted to Cu K α_1 only. For low intensity peaks, a Savitsky–Golay filter was applied for an 11–20 point spread over the peak range of interest. Where adjacent peaks overlapped, a mathematical modeling was performed to deconvolute them. The resulting peak statistics were used to identify the orientations of the individual phases.

2.2 Scanning Electron Microscopy

To analyze surface structure, a Zeiss Auriga 60 Field Emission-SEM (FE-SEM) was used to collect SEM images of a single nucleation layer and of a single PZT volume layer, both deposited on {111}-textured Pt. Images were also obtained for the nucleation layer and the volume-PZT layer on Ti-seed/{111}-Pt for both the post-annealed Ti and as-deposited Ti-seed cases. The images were captured with magnifications of 15 to 35 k \times , electron gun accelerating voltage of 2 kV, extraction voltage of 3.83 kV, filament current of 2.239 A, cathode-to-sample working distance of 3.5 ± 0.5 nm, aperture size of 30 μm , $N = 10\text{--}25$ line averages, and 0.2/0.8 for the ratio of SE2 (far)/In-Lens (near) secondary electron (SE) detection rates in the SEM's annular In-Lens SE detector system.

2.3 Wafer Processing and Capacitance, Polarization and Leakage Measurements

All of the electrical measurements were made in the voltage range of $-10 \text{ V} \leq V \leq 10 \text{ V}$. The PZT thicknesses obtained (Table 1, PZT Vol. column) were used to compute the electric field (E-field) that a sample was subjected to during the electrical measurements. Capacitance and loss tangent as a function of voltage were obtained using an Agilent 4192A 5 Hz–13 MHz LF impedance analyzer. Polarization versus voltage measurements were performed on a Radiant Technologies Inc. Precision Premier II, precision materials analyzer. Four polarization versus voltage/E-field (PE) curves were generated. A bipolar positive PE curve was generated for 0 to 10 to -10 to 0 V. A unipolar positive PE curve was generated for 0 to 10 to 0 V. A bipolar negative PE curve was generated for 0 to -10 to 10 to 0 V. Finally, a unipolar negative PE curve was generated for 0 to -10 to 0 V. The leakage current was measured using a Keithley 2400 source meter. First, the current was measured for 0 to 10 V, then V was set to zero, and then the current was measured for 0 to -10 V.

3. Discussion

3.1 X-ray Diffraction Analysis

Sample characterization and analyses are summarized in Table 2. The table shows identified perovskite PZT peaks from the $\text{PbZr}_{0.52}\text{Ti}_{0.48}\text{O}_3$ International Centre on Diffraction Data (ICDD) #33-0784 data card;¹¹ the quantity of unidentified (Ui) peaks of other phase(s) present; the range of breakdown voltages (V-breakdown) observed for measurements on about five test structures around the wafer; the average of the breakdown voltages measured; the dielectric constant (Epsilon) and loss tangent (tan delta) for DC $V = E = 0$ and $V = \pm 10$ V ($\sim \pm 200$ kV/cm); the maximum $I(+)$ and minimum $I(-)$ leakage current at maximum and minimum voltage, 10 and -10 V, respectively, or at breakdown; and the maximum polarization (Pmax) at maximum voltage of 10 V (~ 200 kV/cm).

For reference, all of the plots from which the XRD peaks were obtained are in Appendix A. The Pt 111 and Si 400 are darkened over in the figures because they are not relevant, but the Pt 222 peak was observed for reference and therefore included in the indexing analysis. Referring to the XRD columns in Table 2, the desired perovskite 001 PZT peaks are observed for all of the samples for which PZT was sputtered (all samples except Sample 6, which is excluded because, for that case, only the nucleation layer was deposited on the Pt). Additional perovskite PZT orientations are of much lower intensity. There are many additional peaks that are unidentified that occur for Samples 1, 6, and 15 (5–6 unidentified peaks), and some of these are notably strong (U4 and U7). The nucleation layer alone (Sample 6) has four unidentified peaks but no perovskite PZT peaks. These three samples did not have a Ti-seed layer. A small unidentified peak named U4 occurs near $2\theta = 30^\circ$ for Samples 3, 20, 21, and 18, all of which have an annealed Ti seed layer.

3.2 SEM Image Analysis

SEM analyses of the V, N, N/S, N/S(A), V/N/S, and V/N/S(A) samples were explored. For the V sample 1-12084 (Fig. 2), large circular features (700–800 nm diameter in size) were observed in the plan view. These large features were generally isolated and distributed within a smaller grain (100–200 nm diameter) matrix. Bright isolated grains about 100-nm in diameter appeared on a dark matrix of similarly sized grains for the N sample 6-12181 (Fig. 3). The various grain types of the observed bimodal microstructures may correspond to the unidentified phases and the perovskite phase determined by XRD for these samples. Higher resolution crystallographic analysis methods such as combined electron diffraction and

transmission electron microscopy (TEM) analyses could prove useful in developing a better understanding, particularly if the material in these regions is oriented. For Figs. 4a and b compare samples N/S and N/S(A), respectively, analyzed by SEM only and not included in Tables 1 and 2, but prepared *in vacuo*. These show a clear difference in the prominence of the grain boundaries for the annealed N/S(A) sample. The difference in microstructure could be related to a difference in phase formation in the two samples. Figs. 5a and b compare samples V/N/S and V/N/S(A), respectively, revealing similar bimodal microstructures with light faceted grains in a matrix of darker equiaxed grains. The N/S(A) structure exhibits a larger grain size for both grain types and an increase in void size distributed along the grain boundaries. It is possible that the different (faceted vs. equiaxed) grains correlate to different phases or grain orientations, but TEM would be required to make this determination.

Table 2 XRD and electrical analyses

Sample ID	Name	Identified PZT peaks	Quantity of unidentified peaks	V-Breakdown Range (V)	V-Breakdown Average (V)	ϵ E = 0	ϵ E = ± 200 kV/cm	$\tan \delta$ E = 0	$\tan \delta$ E = ± 200 kV/cm	Leakage I(+), A	Leakage I(-), A	Pmax ($\mu\text{C}/\text{cm}^2$)
1-12084	V	{001}, 222? No 111 present.	6	0 to 25	13	58.6	57	0.005	0.005	200n	(-6u)	2
6-12181	N	None	4
15-11831	V/N	{001}, 101/110, {111}, 022/220	5	42 to 58	47	136	135	0.01	0.01	40p	(-500p)	1
5-12175	V/S	{001}, 101/110, {111}, 022/220	0	22 to 28	25	1250	480	0.02	0.008	100p	(-300p)	35
2-12174	V/S(A)	{001}, 101/110, {111}, 022/220	0	7 to 22	18	1017	448	0.018	0.009	100p	(-500p)	35
4-12172	V/N/S	{001}, 101/110	0	12 to 24	17	1185	490	0.02	0.014	20n (BD)	(-10n)	35
3-12077	V/N/S(A)	{001}, 101/110, 022/220	1 (U4)	0 to 33	17	1009	480	0.018	0.01	1n (BD)	(-600p)	32
20-12367	V/N/S(A)/ PtB(A)	{001}, 101/110	1 (U4)	17 to 24	21	1000	460	0.018	0.009	270p	(-500p)	31
21-12195	V/N/S/PtB(A)	{001}, 101/110, 022/220	1 (U4)	0 to 24	26	1007	474	0.017	0.009	1n (BD)	(-570p)	32
19-11865	V/N/S/PtB	{001}, 101/110, {111}, 022/220	...	18 to 32	24	1100	460	0.019	0.008	8n	(-60n)	34
18-11873	V/N/S(A)/PtB	{001}, 101/110, {111}, 022/220	1 (U4)	0 to 22	16	940	460	0.018	0.011	350p	(-460p)	34

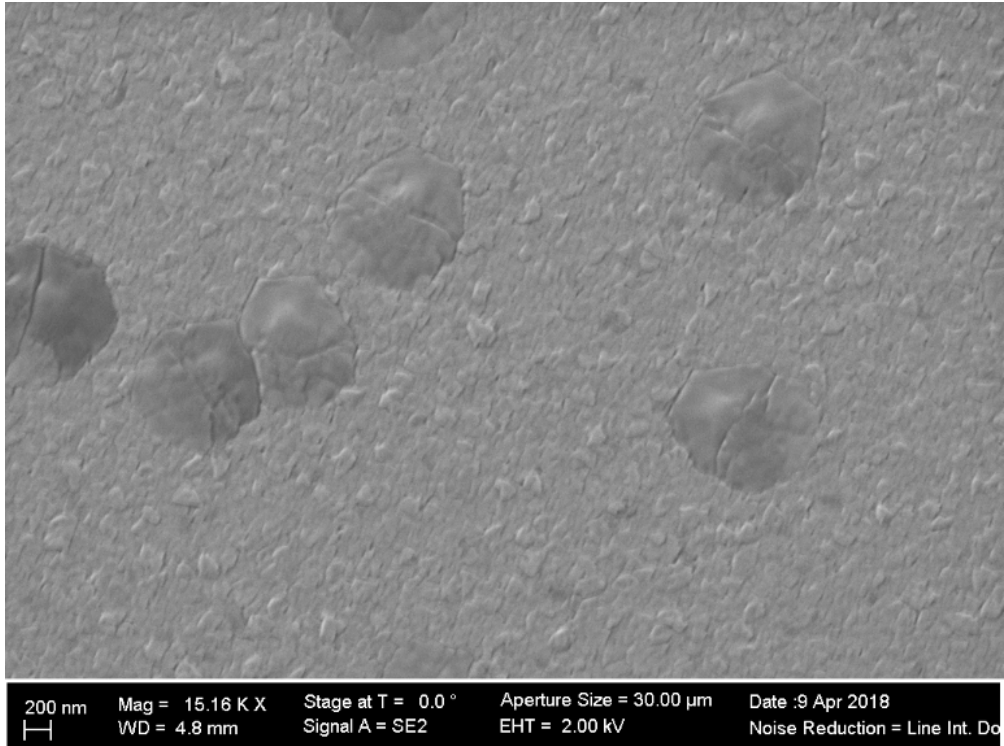


Fig. 2 SEM of 1-12084 volume-only PZT layer on Pt 111 at 15k \times magnification

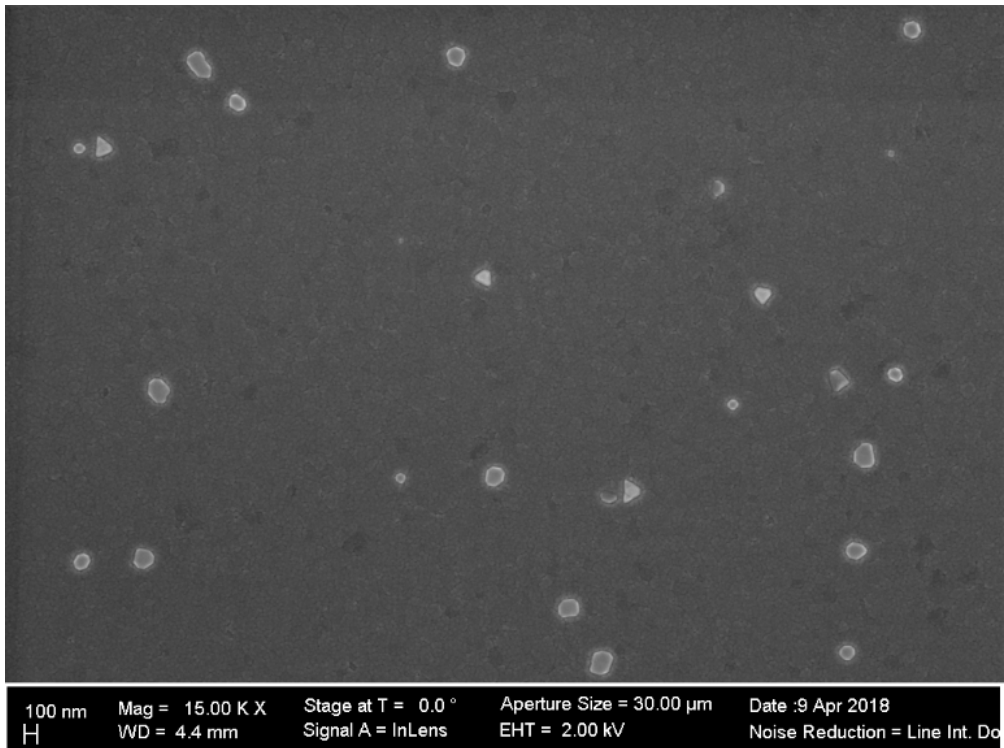


Fig. 3 SEM of 6-12181 nucleation-only layer on Pt 111 at 15k \times magnification

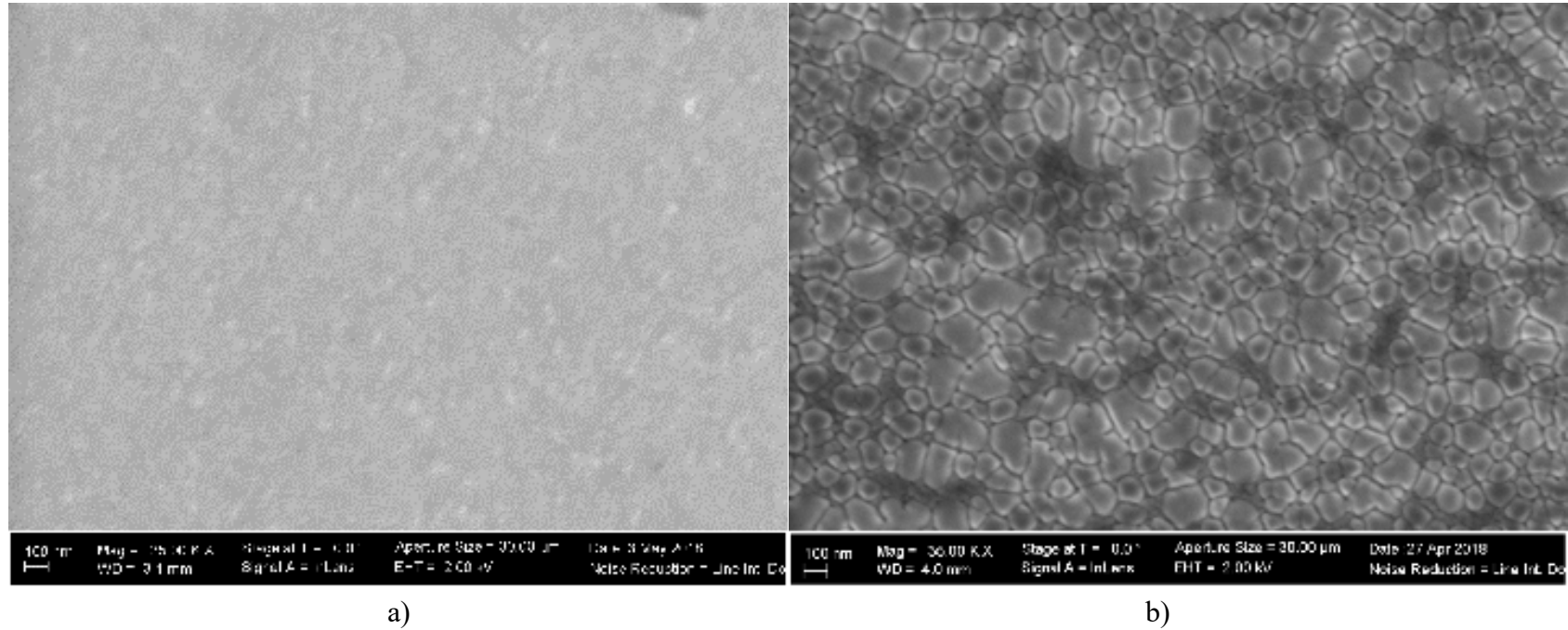


Fig. 4 SEM of nucleation on a) as-deposited and b) annealed Ti seed at 35k \times magnification

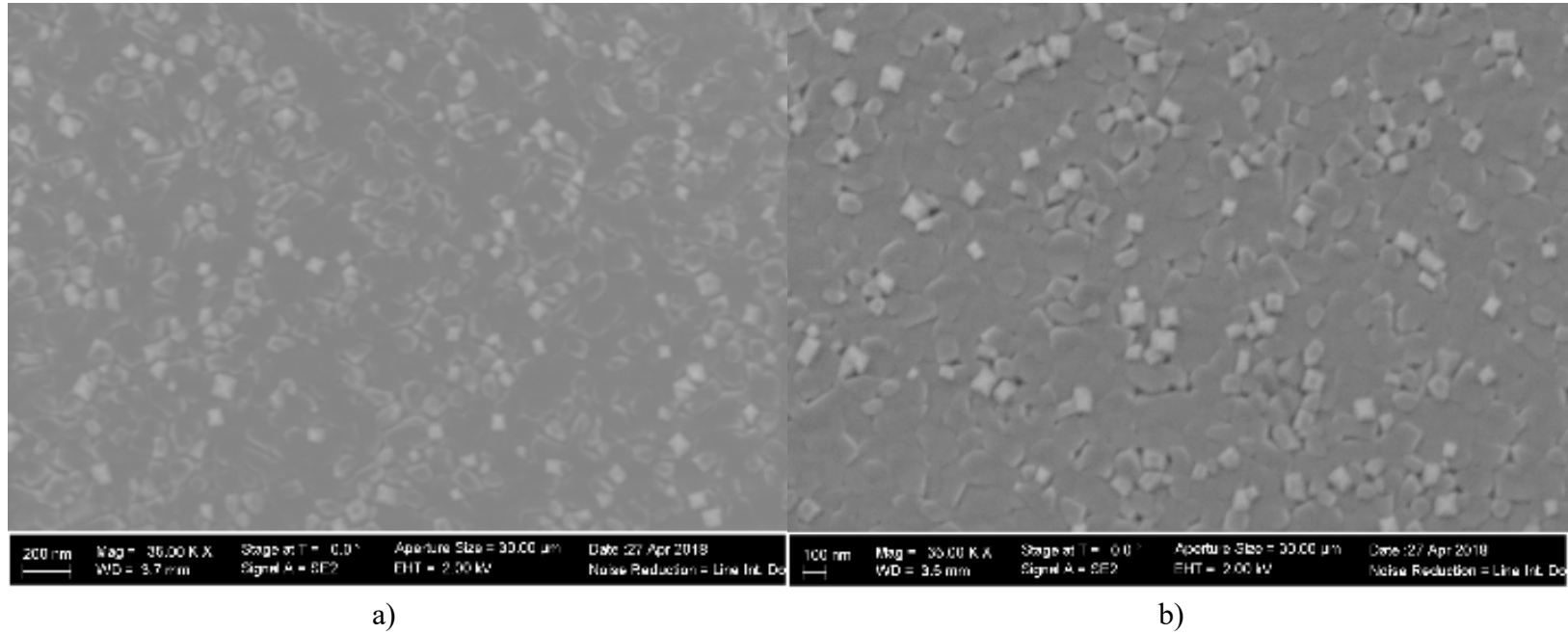


Fig. 5 SEM of volume-PZT/nucleation bilayer on a) as-deposited and b) annealed Ti seed, Samples 4-12172 and 3-12077, respectively, at 35k \times magnification

3.3 Electrical Capacitance, Polarization, and Leakage Current Analyses

For reference, all of the electrical-data plots from which the relevant electrical property values shown in Table 2 were obtained are shown in Appendix B. Referring to Table 2, the highest P_{max} occurred for Samples 5, 2, 4, and 19, though Sample 4 appeared to break down during the I(+) leakage measurement. None of these samples has a U₄ peak in their XRD. The samples with the U₄ XRD peak have slightly lower P_{max} than Samples 5, 2, 4, and 19. Dielectric constants for samples with the U₄ XRD peak are on the low end of the range spanned by those of the previously discussed set of Samples 5, 2, 4, and 19. There does not appear to be any detectable impact of Pt anneal (Anneal 2) on the electrical behavior.

The samples can be divided into three groups. The first group that consisting of a high number and intensity of U_i peaks, Samples 1 and 15, exhibits low dielectric constant, remanent polarization and P_{max}. The reduced properties are consistent with the films consisting primarily of a non-ferroelectric phase(s) such as pyrochlore and PbO. The second group of Samples, 5, 2, 4, and 19, exhibit no U_i peaks and provide the highest dielectric constant, remanent polarization and P_{max}. The third group of samples, Samples 3, 20, 21, and 18, consist primarily of perovskite PZT, but contain a small fraction of U_i peaks. The mixed-phase samples exhibit ferroelectric behavior, but has a reduced (approximately 10%) dielectric constant, remanent polarization, and P_{max} in comparison with the pure perovskite group 2 samples. It is observed that the samples that received the Ti-seed anneal are mostly in group 3, whereas the samples that were not annealed are mostly in group 2. It can be concluded that the Ti-seed anneal is detrimental to the measured electrical properties, but it is a relatively small effect for the properties measured. A broader study on including cross-wafer and wafer-to-wafer reproducibility of properties is warranted.

Comparing leakage measurements for Samples 20, 21, 19, and 18 (see Appendix B), there may be some advantage to the Ti anneal in reducing leakage effects. A larger data set with more measurements across the wafer could help reveal whether there is a statistically valid difference between the two cases. Our research group is interested in the statistics of a broader study of cross-wafer and wafer-to-wafer variation in the electrical measurements and resulting property values. The aim is to seek a path for process improvements that can translate into enhanced electrical performance. We are now in the process of developing autoprobe measurements for testing all available test structures on each wafer, which would maximize sample size for collecting the most complete and reliable data sets.

Two possibilities are considered for the extraneous phases that may be the origin of U_i peaks. The first and most likely is that they are due to pyrochlore. In this case, the unidentified material would not be a ferroelectric phase. Although PTO pyrochlore is well understood and indexed in the ICDD database, PZT pyrochlore is not, though there are studies of it in the literature.¹² A second possibility is that the secondary phase is a highly strained 110 perovskite phase. Reciprocal space maps, which provide the most complete amount of information and are necessary for the analysis of strained films, would be the next logical experimental measurements to perform to prove whether the phase is pyrochlore or perovskite.

4. Conclusion

PZT has been sputter deposited under various conditions and characterized by ellipsometry, XRD, SEM, and ferroelectric and piezoelectric measurements. It was determined that the use of a Ti-seed layer is critical to the sputtered growth of the ferroelectric perovskite PZT. Anneal of the Ti seed layer appears to introduce a phase associated with at least one non-perovskite XRD peak near $2\theta = 30^\circ$ (referred to as U_4 in this study). The data clearly show that the secondary phase formation composes a majority of the film and dominates the electrical properties when the Ti-seed layer is omitted. The use of an annealed Pt surface after a vacuum break did not have a significant impact on PZT phase growth or properties. The wafer-to-wafer phase and property variability appears to be greater than any PtB anneal effect. Further studies of large data sets with autoprobe measurements are in the process of being explored to help inform device performance improvements, repeatability, and reliability.

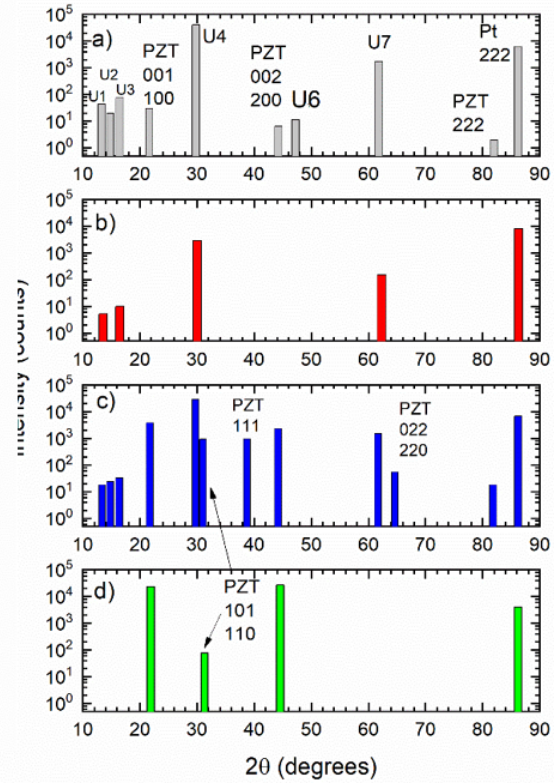
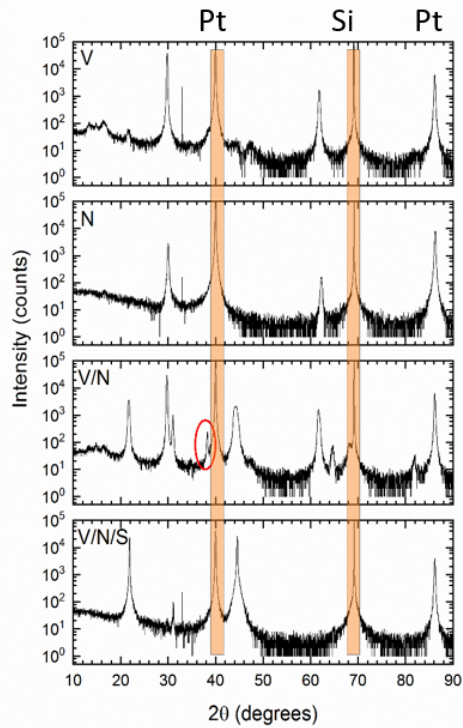
5. References

1. Benoit RR, Rudy RQ, Pulskamp JS, Polcawich RG, Bedair SS. Advances in piezoelectric PZT-based RF MEMS components and systems. *JMM*. 2017;27:083002. <https://doi.org/10.1088/1361-6439/aa710b>.
2. Funakubo H, Dekkers M, Sambri A, Gariglio S, Shklyarevskiy I, Rijnder G. Epitaxial PZT films for MEMS printing applications. *MRS Bulletin*. 2012;37:1030–1038. <https://doi.org/10.1557/mrs.2012.271>.
3. Smith GL, Pulskamp JS, Sanchez LM, Potrepka DM, Proie RM, Ivanov TG, Rudy RQ, Nothwang WD, Bedair SS, Meyer CD, et al. PZT-based piezoelectric mems technology. *J Am Ceram. Soc.* 2012;95(6):1777–1792. <https://doi.org/10.1111/j.1551-2916.2012.05155.x>.
4. Kang MG, Jung WS, Kang CY, Yoon SJ. Recent progress on PZT-based piezoelectric energy harvesting technologies. *Actuators*. 2016;5(1):5. <https://www.google.com/url?sa=t&rct=j&q=&esrc=s&source=web&cd=6&ved=2ahUKEwjw7NCjyqDkAhXJTd8KHdXfALIQFjAFegQIBhAC&url=http%3A%2F%2Fwww.mdpi.com%2F2076-0825%2F5%2F1%2F5%2Fpdf&usq=AOvVaw2ZgHYzekFBukKupmgxaB-v>.
5. Trolrier-McKinstry S, Mural P. Thin film piezoelectrics for MEMS. *J Electroceram* 1. 2004 Jan;12(1–2):7–17.
6. Nguyen MD, Houwman EP, Yuan H, Wylie-van Eerd BJ, Dekkers M, Koster G, ten Elshof JE, Rijnders G. Controlling piezoelectric responses in $\text{Pb}(\text{Zr}_{0.52}\text{Ti}_{0.48})\text{O}_3$ films through deposition conditions and nanosheet buffer layers on glass. *ACS Appl Mater Interfaces*. 2017 Oct 18;9(41):35947–35957. doi: 10.1021/acsami.7b07428.
7. Calame F, Setter N, Mural P. PZT Thin film growth and chemical composition control on flat and novel three-dimensional micromachined structures for MEMS devices [Thesis 3820]. [Lausanne (Fr)]: École Polytechnique Fédérale de Lausanne; 2007, pp. 38–64.
8. Mural P, Maeder T, Sagalowicz L, Hiboux S. Texture control of PbTiO_3 and $\text{Pb}(\text{Zr},\text{Ti})\text{O}_3$ thin films with TiO_2 seeding. *J Appl Phys*. 1998 Jun;83(7):3835–3841. <https://aip.scitation.org/doi/10.1063/1.366614>.
9. Potrepka DM, Mulcahy JR, Polcawich RG, inventors; Process for making lead zirconate titanate (PZT) layers and/or platinum electrodes and products thereof. United States patent US 10,266,936. 2016 Apr 23.

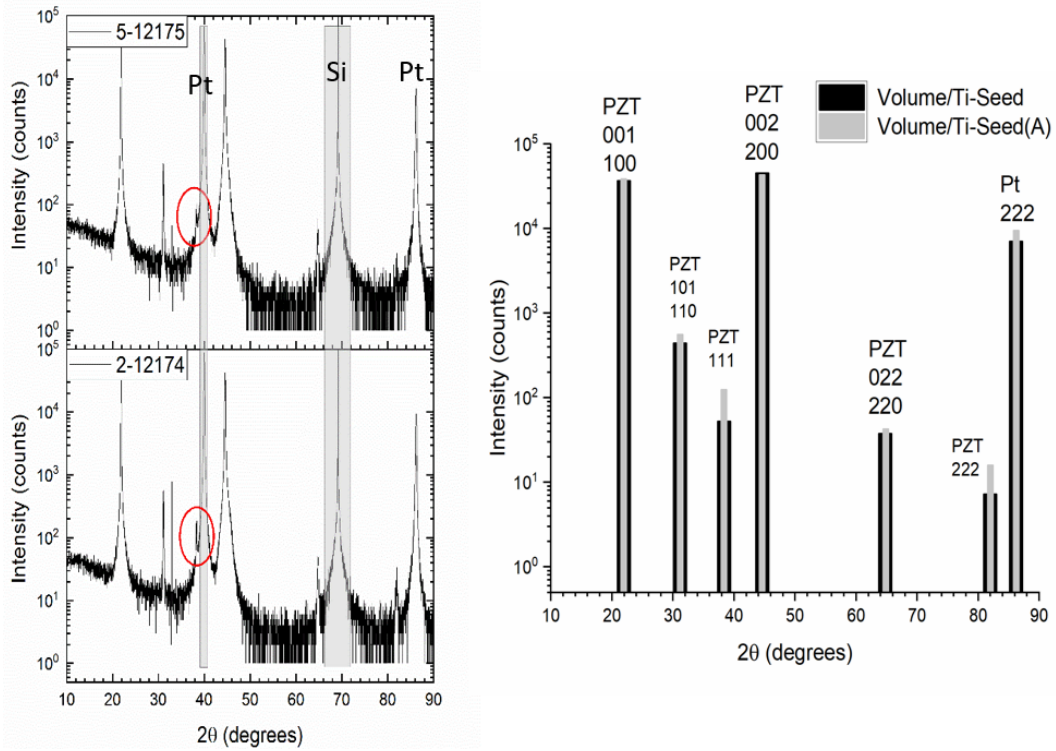
10. Fox GR, Potrepka DM, Polcawich RG. Dependence of {111}-textured Pt electrode properties on TiO₂ seed layers formed by thermal oxidation. *J Mater Sci Mater Electron*. 2018;29:412–426. DOI 10.1007/s10854-017-7930-2. <https://www.springerprofessional.de/dependence-of-111-textured-pt-electrode-properties-on-tio2-seed-/15154944>.
11. The International Centre on Diffraction Data. <http://www.icdd.com/>.
12. Kwok CK, Desu SB. Pyrochlore to perovskite phase transformation in sol-gel derived lead-zirconate-titanate thin films. *Appl Phys Lett*. 1992 Mar;60(12):1430–1432.

Appendix A. X-ray Diffraction Figures

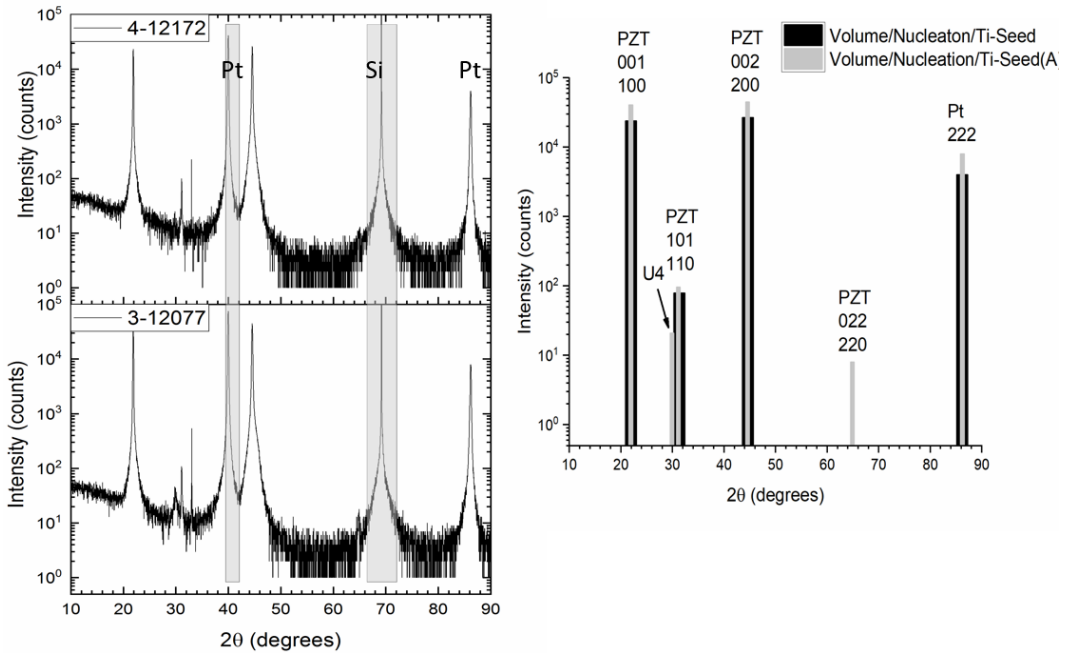
1-12084-E16-02, $t(\text{PZT}) = 4082.6 \text{ \AA}$, V
 6-12181, $t(\text{nucleation}) \sim 300 \text{ \AA}$, N (NOTE: no electrical data)
 15-11831-F11-02, $t(\text{PZT}) = 11172 \text{ \AA}$, V/N
 4-12172, $t(\text{PZT}) = 4816.0 \text{ \AA}$, V/N/S



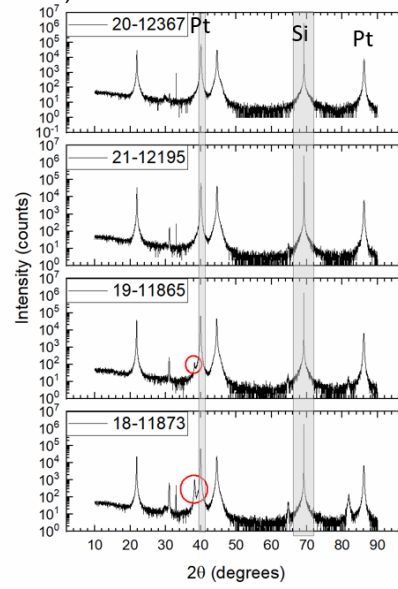
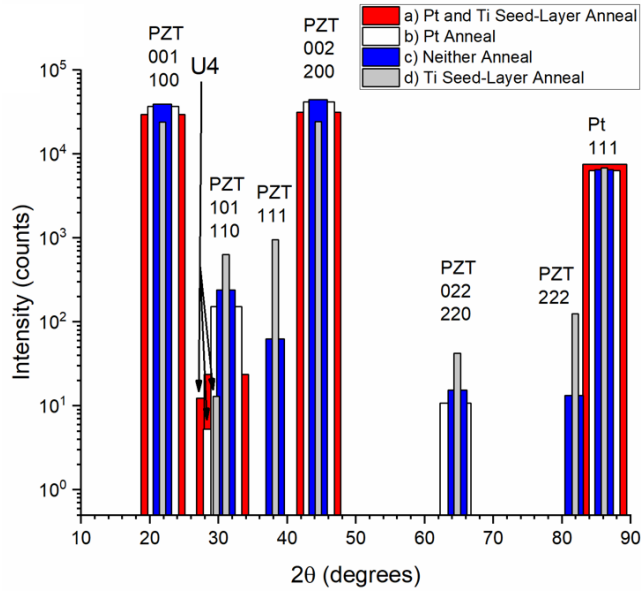
5-12175-E11-02, $t(\text{PZT}) = 5047.5 \text{ \AA}$, V/S
 2-12174-F03-02, $t(\text{PZT}) = 4556.6 \text{ \AA}$, V/S(A), S Annealed



4-12172-D10-02, $t(\text{PZT}) = 4816.0 \text{ \AA}$, V/N/S
 3-12077-F04-02, $t(\text{PZT}) = 4843.0 \text{ \AA}$, V/N/S(A), S Annealed

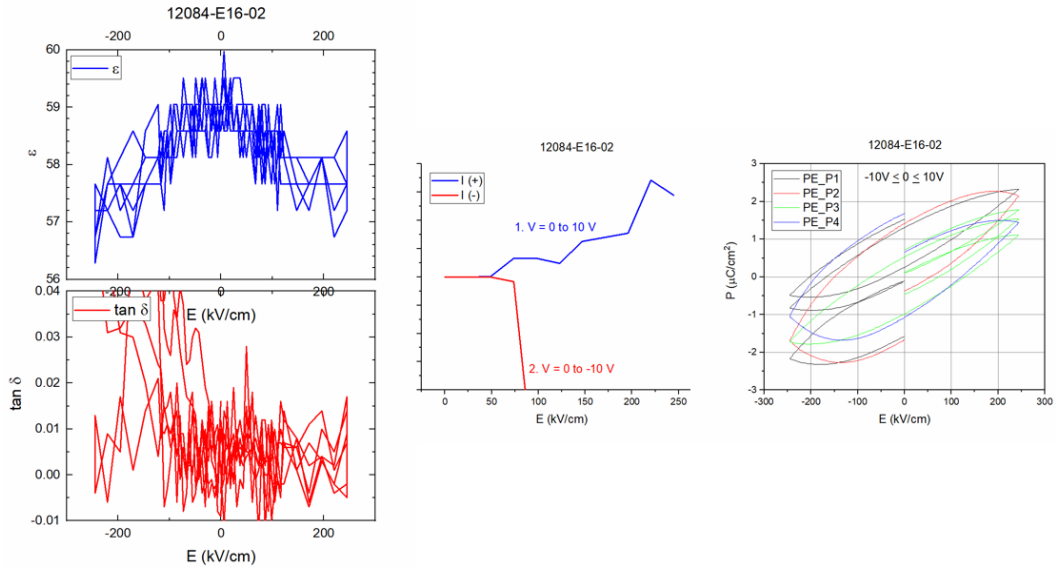


- a) 20-12367-E04-02, $t(\text{PZT}) = 4772.9 \text{ \AA}$, V/N/S(A)/Pt(A), Pt Annealed, S Annealed
- b) 21-12195-G04-03, $t(\text{PZT}) = 4734.0 \text{ \AA}$, V/N/S/Pt(A), Pt Annealed, No S Anneal
- c) 19-11865-F13-02, $t(\text{PZT}) = 4805.6 \text{ \AA}$, V/N/S/Pt, No Pt Anneal, No S Anneal
- d) 18-11873-F04-03, $t(\text{PZT}) = 4867.5 \text{ \AA}$, V/N/S(A)/Pt, No Pt Anneal, S Annealed

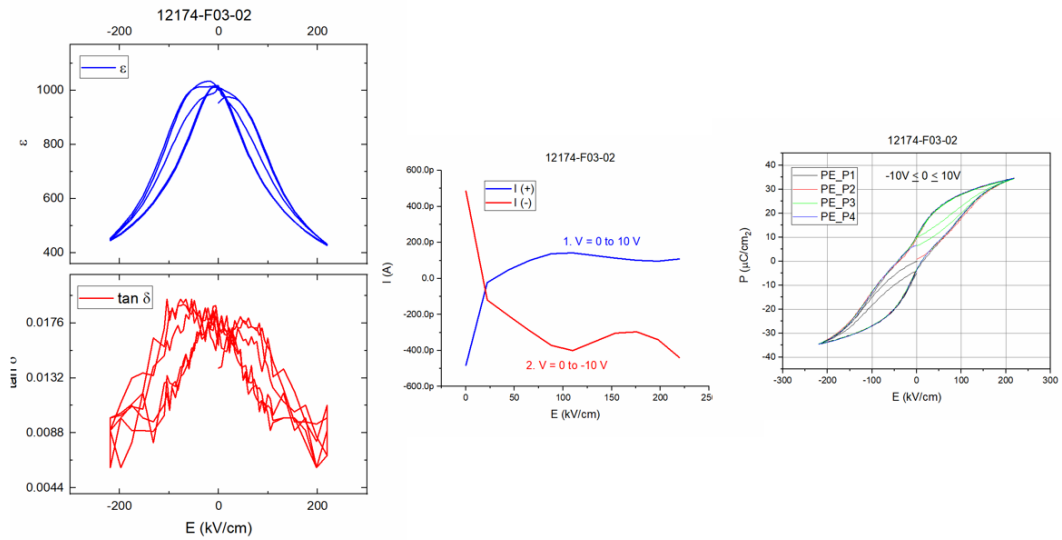


Appendix B. Electrical-Measurement Figures

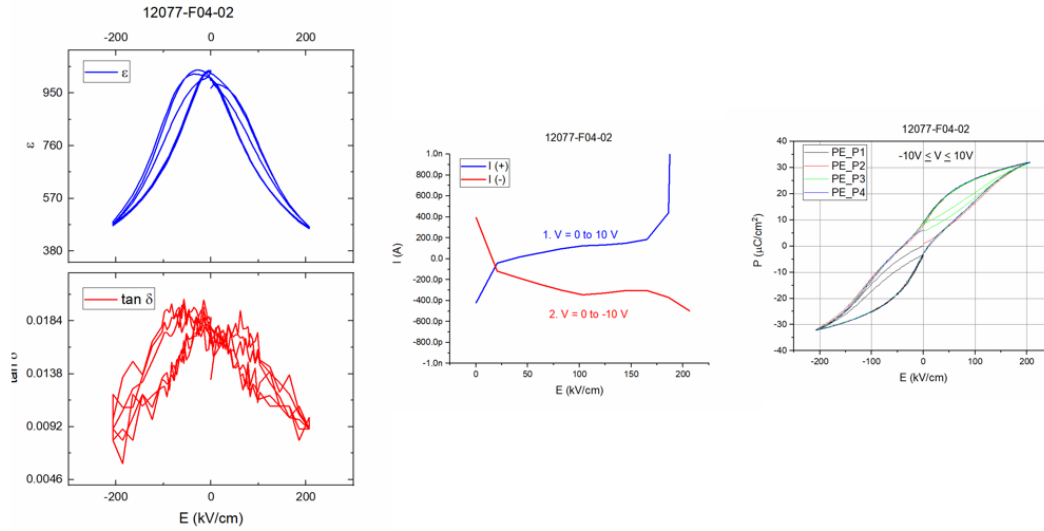
1-12084-E16-02, $t(\text{PZT}) = 4082.6 \text{ \AA}$, V



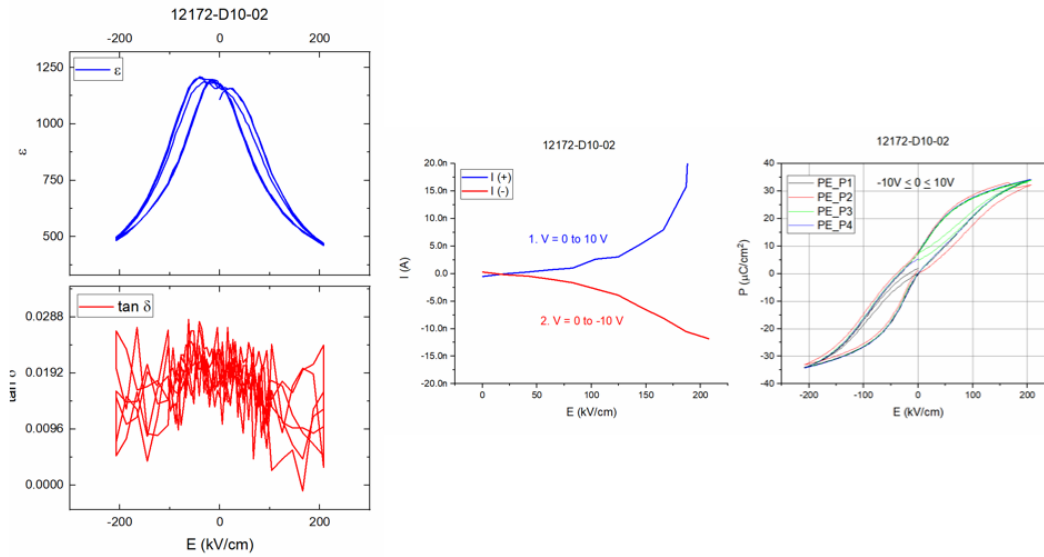
2-12174-F03-02, $t(\text{PZT}) = 4556.6 \text{ \AA}$, V/S(A), S Annealed



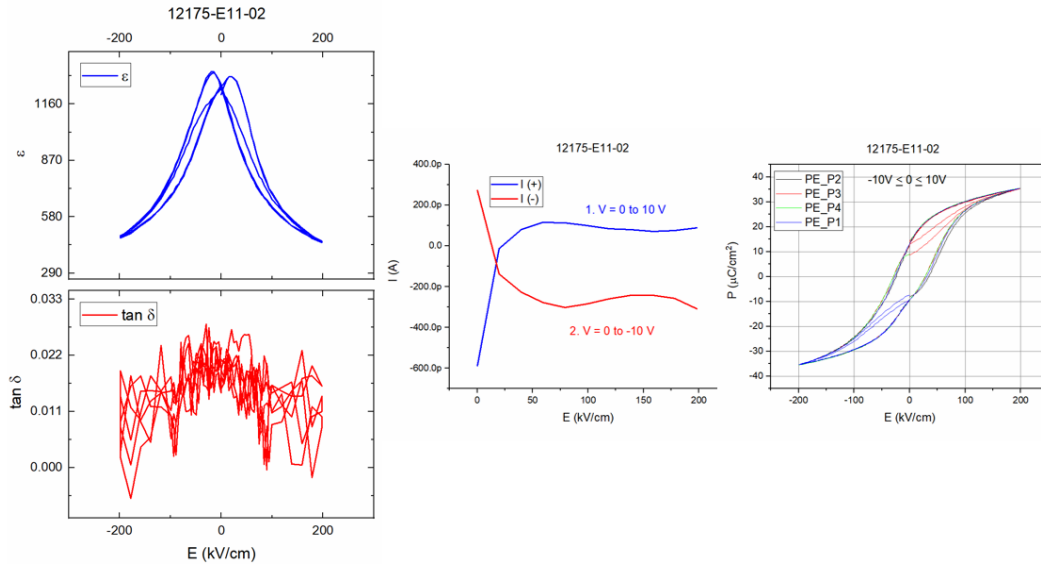
3-12077-F04-02, $t(\text{PZT}) = 4843.0 \text{ \AA}$, V/N/S(A), S Annealed



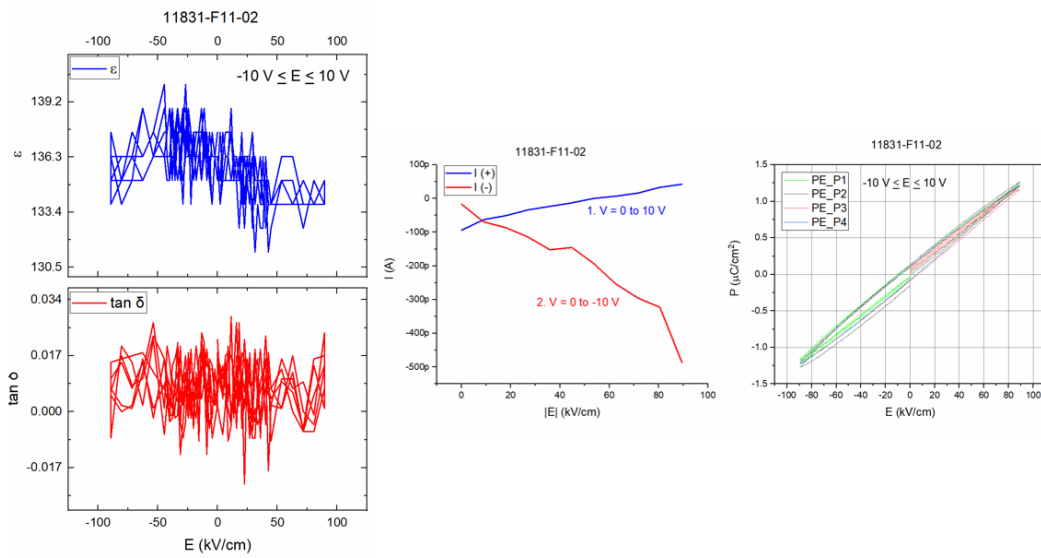
4-12172-D10-02, $t(\text{PZT}) = 4816.0 \text{ \AA}$, V/N/S



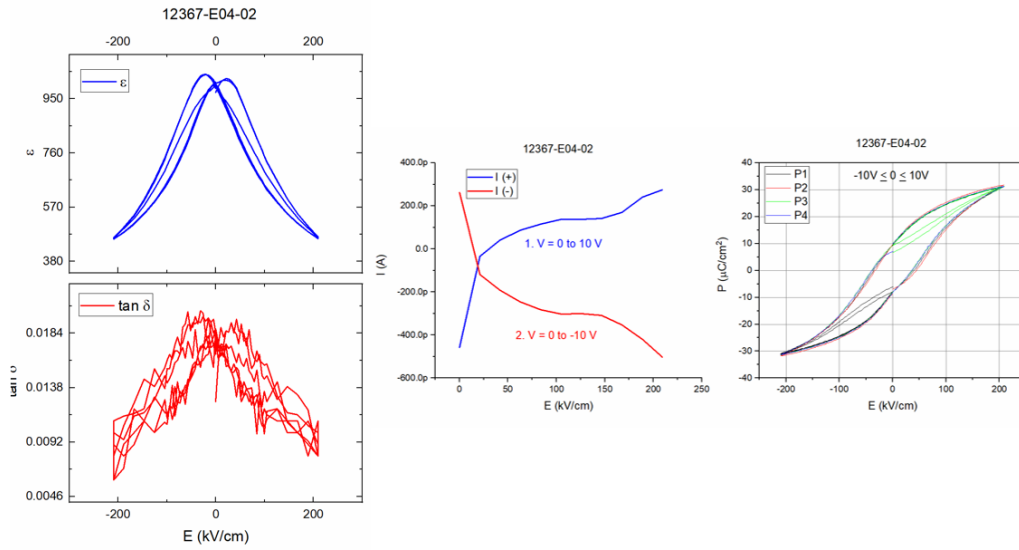
5-12175-E11-02, $t(\text{PZT}) = 5047.5 \text{ \AA}$, V/S



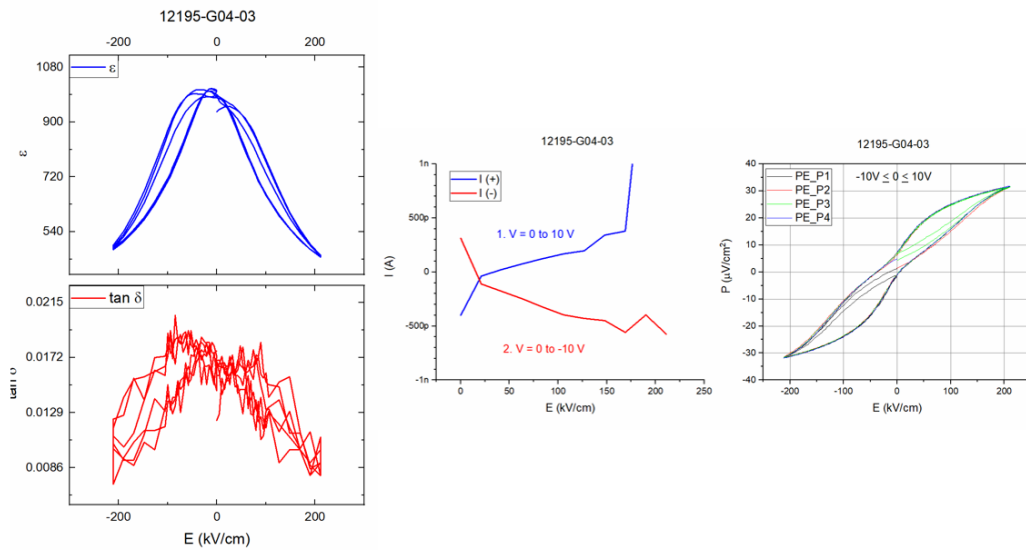
15-11831-F11-02, $t(\text{PZT}) = 11172 \text{ \AA}$, V/N



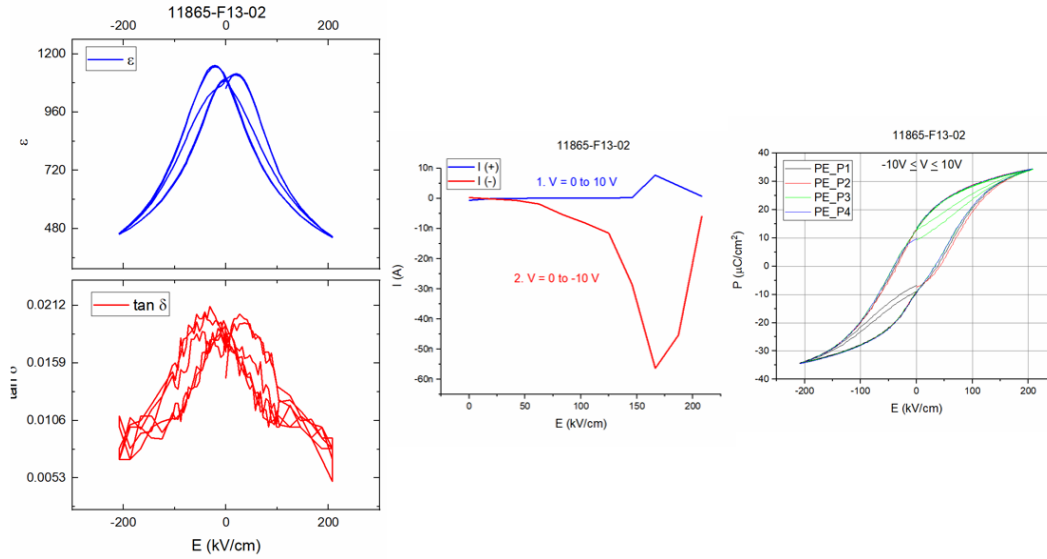
20-12367-E04-02, $t(\text{PZT}) = 4772.9 \text{ \AA}$, V/N/S(A)/Pt(A), Pt Annealed, S Annealed



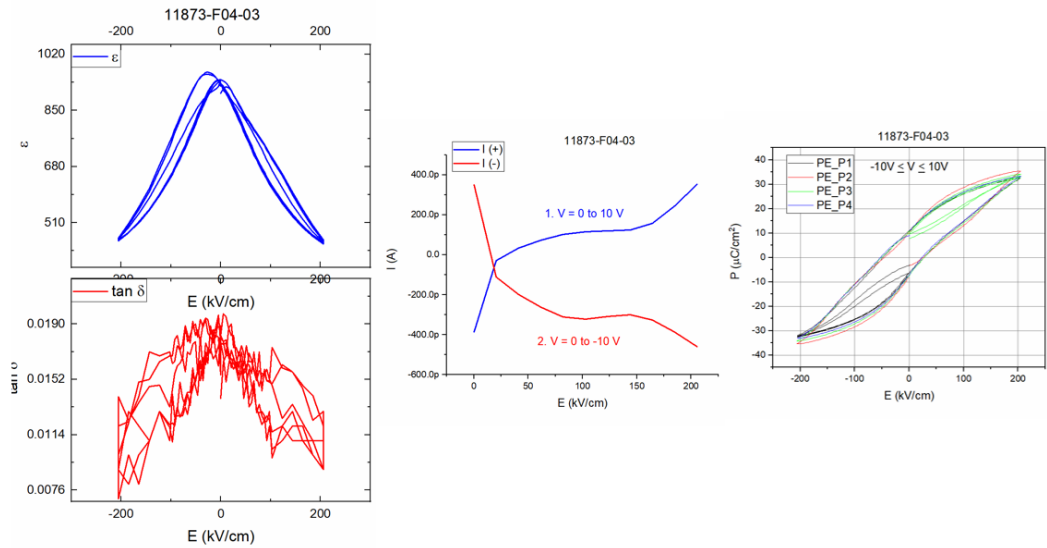
21-12195-G04-03, $t(\text{PZT}) = 4734.0 \text{ \AA}$, V/N/S/Pt(A), Pt Annealed, No S Anneal



19-11865-F13-02, $t(\text{PZT}) = 4805.6 \text{ \AA}$, V/N/S/Pt, No Pt Anneal, No S Anneal



18-11873-F04-03, $t(\text{PZT}) = 4867.5 \text{ \AA}$, V/N/S(A)/Pt, No Pt Anneal, S Annealed



List of Symbols, Abbreviations, and Acronyms

ϵ	(real) dielectric constant
Ar	argon
Au	gold
C	capacitance
Cr	chromium
CV	capacitance
E	E-field derived from the applied voltage divided by the PZT film thickness
E-field	electric field
FE-SEM	field emission-scanning electron microscope
I(+)	leakage current for applied voltage $0 \leq V \leq 10$ V
I(-)	leakage current for applied voltage $0 \leq V \leq 10$ V
ICDD	International Centre on Diffraction Data
ID	identification
N	nucleation sputtered thin film layer
N/S	nucleation layer deposited on the Ti seed
O ₂	oxygen
P	polarization
PbO	lead oxide
PE	polarization versus E-field
piezoMEMS	piezoelectric microelectromechanical system
P _{max}	maximum polarization
Pt	platinum
Pt(A)	annealed platinum
PtB	Pt with vacuum breaks
PZT	lead zirconate titanate

RF	radio frequency
S	Ti seed sputtered thin film layer
S(A)	annealed Ti seed
SE	secondary electron
SEM	scanning electron microscope
Si	silicon
SiO ₂	silicon dioxide
tan δ	loss tangent
TEM	transmission electron microscope
Ti	titanium
TiO ₂	titanium dioxide
U _i	collectively the unidentified X-ray peaks
V	PZT volume sputtered thin-film layer
V/N	PZT volume deposited on the nucleation layer
V/N/S	PZT volume film (the main portion of the final thin film) deposited on the nucleation layer deposited on the Ti seed layer
V/S	PZT volume deposited on the Ti seed layer
U ₁ , U ₂	the individual unidentified X-ray peaks indexed in the X-ray diffraction scans
XRD	X-ray diffraction

Glossary

Ex-situ method samples removed from vacuum to perform another task or tasks, such as a furnace anneal outside of the sputtering equipment

In vacuo method a method of processing without a vacuum break

For PZT pyrochlore, no ICDD standard reference exists and published reports are not standardized yet (see, for example, Kwok and Desu¹²) and is not considered here.

1 DEFENSE TECHNICAL
(PDF) INFORMATION CTR
DTIC OCA

1 CCDC ARL
(PDF) FCDD RLD CL
TECH LIB

11 CCDC ARL
(PDF) FCDD RLS
R D DELROSARIO
FCDD RLS RL
C J MORRIS
J S PULSKAMP
R Q RUDY
R R BENOIT
J L MARTIN
B K POWER
S K ISAACSON
J M PUDER
D M POTREPKA
FCDD RLS E
N A STRNAD